Fate of entanglement in magnetism under Lindbladian or non-Markovian dynamics and conditions for their transition to Landau-Lifshitz-Gilbert classical dynamics

Federico Garcia-Gaitan and Branislav K. Nikolić*
Department of Physics and Astronomy, University of Delaware, Newark, DE 19716, USA

The entanglement of many localized spins (LS) within solid magnetic materials is a topic of great basic and applied interest, particularly after becoming amenable to experimental scrutiny where, e.g., very recent neutron scattering experiments have witnessed macroscopic entanglement in the ground state (GS) of antiferromagnets persisting even at elevated temperatures. On the other hand, spintronics and magnonics studies assume that LS of antiferromagnets are in unentangled Néel GS, as well as that they evolve, when pushed out of equilibrium by current or external fields, according to the Landau-Lifshitz-Gilbert (LLG) equation viewing LS as classical vectors of *fixed* length. The prerequisite for applicability of the LLG equation is *zero entanglement* in the underlying many-body quantum state of LS. In this study, we initialize quantum Heisenberg ferro- or antiferromagnetic chains hosing $S = 1/2$, $S = 1$ or $S = 5/2$ LS into unentangled pure state and then evolve them by quantum master equations (QMEs) of Lindblad or non-Markovian type, derived by coupling LS weakly to bosonic bath (due to phonons in real materials) or by using additional "reaction coordinate" in the latter case. The time evolution is initiated by applying an external magnetic field, and entanglement of the ensuing *mixed* quantum states is monitored by computing its negativity. We find that non-Markovian dynamics *never* brings entanglement to zero, in the presence of which the vector of spin expectation value *changes its length* to render the LLG equation *inapplicable*. Conversely, Lindbladian (i.e., Markovian) dynamics ensures that entanglement goes to zero, thereby enabling quantum-to-classical transition in all cases—$S = 1/2$, $S = 1$ and $S = 5/2$ ferromagnet or $S = 5/2$ antiferromagnet—*except* for $S = 1/2$ and $S = 1$ antiferromagnet. Finally, we investigate the stability of entangled antiferromagnetic GS upon suddenly coupling it to bosonic baths.

Introduction.—The fate of entanglement of many interacting quantum spins, localized at the sites of crystalline lattices of magnetic materials [1] or in optical lattices of their quantum simulators [2], under finite temperature or nonequilibrium conditions is a topic of great contemporary interest. For example, recent experiments [3–5] have succeeded to witness [6–8] multipartite entanglement [3, 9] of macroscopically large number of spins hosted by antiferromagnetic insulators (AFIs) in equilibrium up to surprisingly high temperature $T \lesssim 200$ K [3]. Transient entanglement in nonequilibrium AFIs could also be witnessed via very recently proposed schemes [10, 11]. Due to finite temperature and/or nonequilibrium, such systems inevitably generate *mixed entangled* states, also in the focus of our study [Eq. (1)], that are far less understood [12–16] than the pure [2] entangled ones. In computational quantum physics, quantum spin systems are a standard playground for developing algorithms, such as tensor networks (TN) [17], that can efficiently encode ground states (GSs) containing low-entanglement—however, entanglement growth in nonequilibrium [18] poses significant challenge for these algorithms [19] and the role of dissipative environment in limiting the so-called "entanglement barrier" is intensely explored [20]. It is insightful to invoke a pedagogical example of an entangled GS, such as that of AFI chain hosting localized spins (LS) $S = 1/2$, which has been realized experimentally [21] and is described by the Heisenberg Hamiltonian [22] $\hat{H}_H = J\sum_{i=1}^{N-1} \hat{\mathbf{S}}_i \cdot \hat{\mathbf{S}}_{i+1}$. The GS is entangled [9] as it cannot be expressed as the direct product of multiple single-spin states in any basis, as obvious from its form for $N = 4$ sites: $|\mathrm{GS}\rangle_{\mathrm{AFI}} = \frac{1}{\sqrt{12}}\big(2\,|\uparrow\downarrow\uparrow\downarrow\rangle + 2\,|\downarrow\uparrow\downarrow\uparrow\rangle - |\uparrow\uparrow\downarrow\downarrow\rangle - |\uparrow\downarrow\downarrow\uparrow\rangle - |\downarrow\downarrow\uparrow\uparrow\rangle - |\downarrow\uparrow\uparrow\downarrow\rangle\big)$. Its energy, ${}_{\mathrm{AFI}}\langle \mathrm{GS}|\hat{H}|\mathrm{GS}\rangle_{\mathrm{AFI}} = -2J$, is lower than the energy, $\langle \text{Néel}|\hat{H}|\text{Néel}\rangle = -J$ of unentangeled Néel state $|\text{Néel}\rangle = |\uparrow\downarrow\uparrow\downarrow\rangle$, which is the precise meaning behind "quantum spin fluctuations" [23] sintagma. Here $\hat{S}_i^\alpha = \hat{I}_1 \otimes \ldots \otimes S\hat{\sigma}^\alpha \otimes \ldots \otimes \hat{I}_{\mathrm{N_{AFI}}}$ acts nontrivially, as the Pauli matrix $\hat{\sigma}^\alpha$, in the Hilbert space of spin at site i; $\hat{I}_i$ is the unit operator; and $J > 0$ is AF exchange interaction. The expectation value of spin, $\langle \hat{\mathbf{S}}_i \rangle = \langle \mathrm{GS}|\hat{\mathbf{S}}_i|\mathrm{GS}\rangle \equiv 0$, vanishes as a direct consequence [24–26] of non-zero entanglement entropy of AFI GS.

In the case of ferromagnetic insulators (FIs), quantum spin fluctuations [23] are absent [27] and both classical $\uparrow\uparrow \ldots \uparrow\uparrow$ and its unentangled quantum counterpart $|\uparrow\uparrow \ldots \uparrow\uparrow\rangle$ are GS of the respective classical and quantum Hamiltonians. However, excited states of FI chain—such as one-magnon Fock state [28, 29] $|1_q\rangle = \frac{1}{\sqrt{N}}\sum_{n=0}^{N-1} e^{iqx_n}|\underbrace{\uparrow\ldots\uparrow}_{n}\downarrow\ \underbrace{\uparrow\ldots\uparrow}_{N-n-1}\rangle$ where q is the wavevector and $x_n = na$ is the x-coordinate along the chain (with the lattice constant a)—is macroscopically entangled [30, 31], as is the case of multi-magnon states [32]. The robustness of entanglement of such states has been studied for a long time in quantum computing (using analogous multi-qubit states known as W states) [16, 33], as well as more recently in "quantum magnonics" [29] using quantum master equations (QMEs) formulated in second-quantization [34, 35].

On the other hand, it is commonly assumed in an-

tiferromagnetic spintronics [36–40] that GS of AFI is unentangled Néel state; or that excited states (like magnons [41, 42]) of either AFI or FI, as triggered experimentally by injected current [40, 43, 44] or electromagnetic radiation [45–47], are *classical and governed* [43, 48] by the celebrated Landau-Lifshitz-Gilbert (LLG) equation [49–51]. It is also widely-believed that large spin value S [24] and/or room temperature ensure applicability of the LLG equation. This plausible notion is motivated by the eigenvalue of $\hat{\mathbf{S}}_i^2$ operator being $S^2(1+1/S)$, instead of S^2, which suggests that quantum effects become progressively less important for $S > 1$. However, even for single quantum spin the required value of S to match quantum and classical LLG dynamics can be unrealistically large [52, 53] in the presence of magnetic anisotropy (or any quadratic or higher order terms in spin Hamiltonian) [54]. Also, quantum corrections persist for all $S < \infty$ [52, 53], vanishing as $(2S)^{-1}$ in the classical limit [55]. Importantly, most of the standard magnetic materials host LS with rather small $S \leq 5/2$ [56].

The search for a rigorous proof that quantum dynamics of a *single* spin can transition to classical LLG dynamics, due to interaction with dissipative environment like the bosonic bath and conditions imposed on it, has a long history dating back to archetypical spin-boson model [57] and recent generalizations [58] completing the proof while also unraveling nature of quantum corrections to classical LLG dynamics. However, such proofs [58] do not explain how quantum dynamics of *many* spins can transition to classical dynamics to be describable by a system of coupled LLG equations [59], often applied without scrutiny to both ferro- and antiferromagnets in spintronics [43] and magnonics [60]. The *key prerequisite* for such a transition is the *absence of entanglement* [24, 25], i.e., the underlying quantum state of many LS must remain unentangled pure $|\sigma_1(t)\rangle \otimes |\sigma_2(t)\rangle \otimes \cdots \otimes |\sigma_N(t)\rangle$, or unentangled mixed [12–16]

$$\hat{\rho}(t) = \sum_n p_n \hat{\rho}_n^{(1)}(t) \otimes \hat{\rho}_n^{(2)}(t) \ldots \hat{\rho}_n^{(N)}(t), \qquad (1)$$

at all times t in order for time evolution of quantum-mechanical expectation values $\langle \hat{\mathbf{S}}_i \rangle$ to be able to transition to the solutions [59] $\mathbf{S}_i(t)$ of coupled LLG equations

$$\langle \hat{\mathbf{S}}_i \rangle(t) \mapsto \mathbf{S}_i(t). \qquad (2)$$

Otherwise, in the entangled quantum state the length of vectors $\langle \hat{\mathbf{S}}_i \rangle(t)$ is changing in time [61] which obviously *cannot be mimicked* by $\mathbf{S}_i(t)$ of *fixed length* [59] in the LLG equation. In Eq. (1), $\hat{\rho}_n^{(i)}$ is the density matrix spin at site i. We consider usage of the LLG equation in the context of atomistic spin dynamics (ASD) [59], where each atom of the lattice hosts one classical vector $\mathbf{S}_i$.

In this Letter, we view AFI and FI as open quantum systems [62–64] by coupling them either: (*i*) weakly to a bosonic bath, assumed to arise due to bosonic quasiparticles in solids such as phonons, whose tracing out allows one to derive [65] the universal Lindblad QME [Eq. (3)]; or (*ii*) strongly to a single bosonic mode which, in turn, interacts weakly with the bosonic bath, so that tracing over both allows us to derive non-Markovian QME within the so-called "reaction coordinate" (RC) method [66]. We monitor the presence of entanglement in the density matrix of all LS $\hat{\rho}(t)$ via entanglement negativity $E_N(t)$ [12–16], and we concurrently compare quantum $\langle \hat{\mathbf{S}}_i \rangle(t)$ vs. classical $\mathbf{S}_i(t)$ trajectories in Figs. 1–3.

Models and methods.—We consider FI ($J < 0$) or AFI ($J > 0$) chain modelled by the Heisenberg Hamiltonian $\hat{H}_H$, which can include interaction with a homogeneous external magnetic field switching on for $t \geq 0$, $\hat{H} = \hat{H}_H - \sum_i g\mu_B \mathbf{B}_{\rm ext}(t \geq 0) \cdot \hat{\mathbf{S}}_i$, where g is the gyromagnetic ratio and μ_B is the Bohr magneton. We set $\hbar = 1$ and $k_B = 1$. These models of realistic magnetic materials [3, 21] are made open quantum systems by coupling them bosonic baths, so that the total Hamiltonian becomes $\hat{H}_{\rm tot} = \hat{H} + \hat{H}_{\rm bath} + \hat{V}$. Here $\hat{H}_{\rm bath}$ models a set of independent baths, one per each spin [65, 67], as harmonic oscillators [57], $\hat{H}_{\rm bath} = \sum_{ik} w_{ik} \hat{a}_{ik}^\dagger \hat{a}_{ik}$, using an operator $\hat{a}_{ik}(\hat{a}_{ik}^\dagger)$ which annihilates (creates) a boson in mode k. The boson interacts with spin operator at site i [62] via $\hat{V} = \sum_k g_k \sum_i \hat{\mathbf{S}}_i(\hat{a}_{ik} + \hat{a}_{ik}^\dagger)$, where g_k are the coupling constants. By assuming small g_k, QME of the Lindblad type [68, 69] can be derived by tracing out the bosonic bath and by expanding the resulting equation to second order. Rather than relying on traditional approaches for the derivation of the Lindblad QME—such as using Born, Markov and secular approximations [66, 68, 70]—we follow the procedure of Ref. [65] for universal Lindblad QME which evades difficulties of the secular approximation [71]. For example, for systems with (nearly) degenerate eigenstates, as is the case of FI and AFI models considered, secular approximation leads to improperly derived [70] Lindblad QME for LS because of assuming that energy splitting is much bigger than fluctuations due to the bath. The same problem was addressed in a number of recent studies [72, 73], besides the resolution offered in Ref. [65].

The universal Lindblad QME [65] considers a single Lindblad operator $\hat{L}_i$ for each spin, so that only N such operators are needed to obtain

$$d\hat{\rho}/dt = -i[\hat{H}, \hat{\rho}] + \sum_i^N \hat{L}_i \hat{\rho} \hat{L}_i^\dagger - \frac{1}{2}\{\hat{L}_i^\dagger \hat{L}_i, \hat{\rho}\}, \qquad (3)$$

where we also ignore typically negligible Lamb-shift corrections [66] to the Hamiltonian. The Lindblad QME is time-local due to the assumption that bath-induced changes to the system dynamics are slow relative to the typical correlation time of the bath. We compute $\hat{L}_i$ operators as a power series (where we use cutoff $N_L \leq 20$)

$$\hat{L}_i = \sum_{n=0}^{N_L} c_n (\mathrm{ad}_{\hat{H}})^n [\hat{\mathbf{S}}_i], \quad c_n = \frac{(-i)^n}{n!} \int_{-\infty}^{\infty} dt g(t) t^n, \quad (4)$$

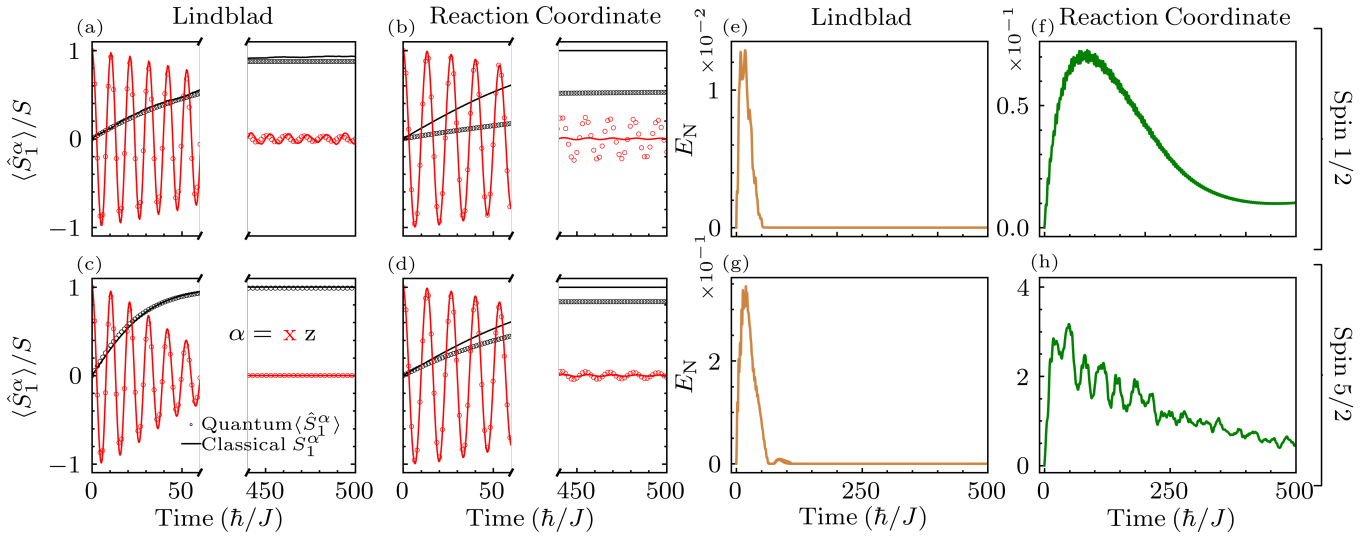

FIG. 1. Time-dependence of QME-computed $\langle \hat{S}_1^\alpha \rangle(t)$ vs. classical-LLG-computed $S_1^\alpha(t)$ of LS (a),(b) $S = 1/2$ or (c),(d) $S = 5/2$ on site $i = 1$ of FI chain of $N = 4$ sites. (e)–(h) Time dependence of entanglement negativity [12] $E_N(t)$ between two halves of FI chain in the case of quantum evolution (circles) in panels (a)–(d). The LS open quantum system evolution is conducted using either Lindblad (i.e., Markovian) or RC (i.e., non-Markovian) QME with bosonic bath temperature $T = |J|$.

thereby evading the need for exact diagonalization [65] of FI or AFI Hamiltonians. Here $\mathrm{ad}_{\hat{H}}[X] = [\hat{H}, X]$ and the jump correlator function is defined via the Fourier transform of the spectral function of the bath, $J(\omega) = 2\pi \sum \delta(\omega - \omega_k)$, as $g(t) = \frac{1}{\sqrt{2\pi}} \int_{-\infty}^{\infty} d\omega \sqrt{J(\omega)} e^{-i\omega t}$. For numerical calculations, we considered an Ohmic [58] spectral function with a rigid ultraviolet cutoff

$$J(\omega) = \frac{\Gamma \omega}{\omega_m} n_{\mathrm{BE}}(\omega) \Theta(\omega_m - \omega), \tag{5}$$

where Γ is the reorganization energy representing the magnitude of fluctuations and dissipation; ω_m characterizes how quickly the bath relaxes towards equilibrium; $n_{\mathrm{BE}}(\omega)$ the Bose-Einstein distribution; and Θ is the Heaviside step function.

The Lindblad QME [Eq. (3)] is only valid for a weak system-bath coupling, as it assumes a second order truncation in g_k. Since this is not always the case, several approaches [62, 64] exist to treat strong system-bath coupling, such as polaron, star-to-chain and thermofield transformations [74], and the RC method [71]. The RC method we employ is based on the Bogoliubov transformation, and it allows one to construct a new bosonic mode $\hat{b}$ called the RC. This mode is coupled strongly to the system, but weakly to a residual bosonic bath, while conserving the bosonic commutation relations. The new Hamiltonian of the system then becomes

$$\hat{H}_{\mathrm{tot}} = \hat{H} + \lambda \sum_i \hat{\mathbf{S}}_i (\hat{b} + \hat{b}^\dagger) + \Omega \hat{b}^\dagger \hat{b} + \hat{H}_{\mathrm{RC\text{-}B}} + \hat{H}_{\mathrm{bath}}, \tag{6}$$

where λ is the strength of the coupling between the RC and the system; Ω is the frequency of the RC; $\hat{H}_{\mathrm{RC\text{-}B}} = \sum_{k>1} \tilde{g}_k (\hat{b} + \hat{b}^\dagger)(\hat{c}_k + \hat{c}_k^\dagger)$ is the RC-bath coupling Hamiltonian; and $\hat{H}_{\mathrm{bath}}$ is the bosonic bath Hamiltonian considered to be identical to the case used in derivation of Eq. (3), but with one less bosonic mode and with properly transformed coupling coefficients. Thus, the parameters λ and Ω are expressed [75] in terms of the parameters in Eq. (5), $\lambda^2 = \frac{1}{6\pi} \sqrt{\frac{5}{3}} \Gamma \omega_m$ and $\Omega = \sqrt{\frac{5}{3}} \omega_m$, while the spectral function of the residual bath

$$J'(\omega) = \frac{2\sqrt{5/3} \pi \omega \omega_m^2 n_{\mathrm{BE}}(\omega)}{3 \left[\pi^2 \omega^2 + 4\omega \operatorname{arctanh}(\omega/\omega_m) (\omega \operatorname{arctanh}(\omega/\omega_m) - 2\omega_m) + 4\omega_m^2 \right]}, \tag{7}$$

is independent of the original coupling strength Γ. This allows us to derive QME which has the same form as Eq. (3), but it uses $\hat{H} \mapsto \hat{H} + \lambda \sum_i \hat{\mathbf{S}}_i (\hat{b} + \hat{b}^\dagger) + \Omega \hat{b}^\dagger \hat{b}$. Since $\lambda \propto \sqrt{\Gamma}$, the coupling of the system to the RC can be arbitrarily strong without affecting coupling to the residual bath. Despite being time-local, this Lindblad

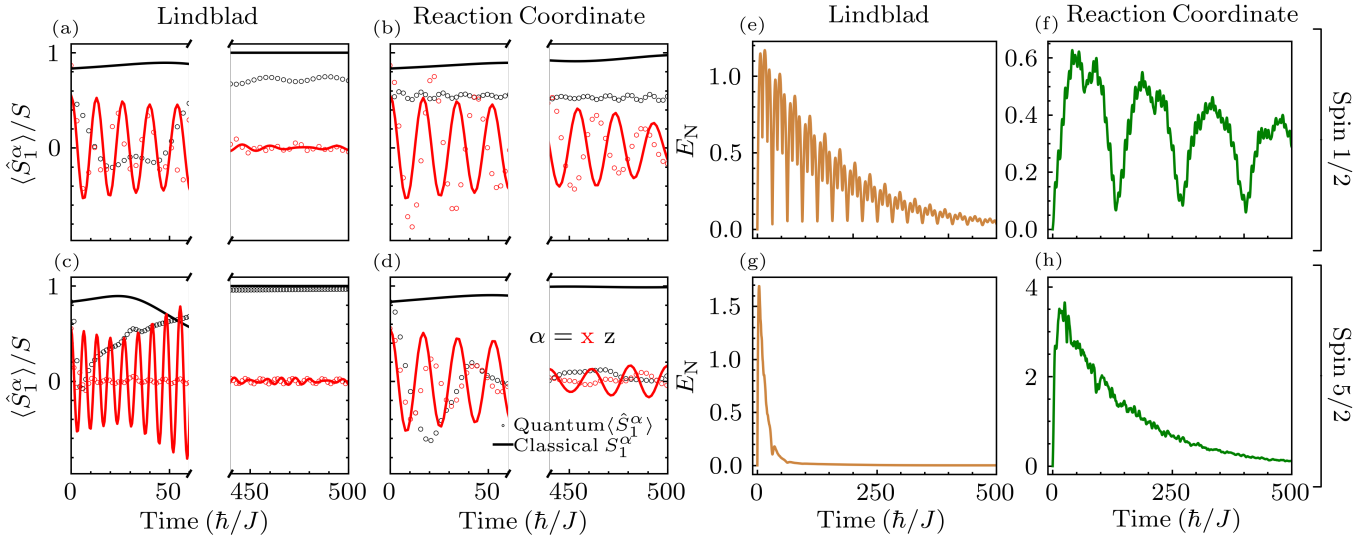

FIG. 2. Panels (a)–(h) are counterparts of Fig. 1(a)–(h), but using AFI chain composed of $N = 4$ sites. Additional cases of AFI or FI chains hosting $S = 1$ LS, or by including their additional interactions (such as easy-axis anisotropy, long-ranged dipole-dipole interaction and Dzyaloshinskii-Moriya interaction) are provided in the SM [74].

QME including RC captures non-Markovian effects [76]. They, otherwise, require integro-differential QMEs with time-retarded kernel [62–64]. In order to reduce computational complexity for many LS, an effective Hamiltonian was built by considering [76] only the lowest energy states of the RC, i.e., the matrix representation of $\hat{b}$ is truncated to finite size 15×15.

Results and discussion.—We solve Eq. (3) for Lindbladian dynamics, as well as for non-Markovian dynamics when the RC is included in the Hamiltonian, for FI and AFI chains composed of $N = 4$ sites with periodic boundary conditions hosting spins $S = 1/2$ or $S = 5/2$, as well as $S = 1$ in the Supplemental Material (SM) [77]. The two QMEs are solved using the fourth order Runge-Kutta method, where $|J| = 1$ sets the unit of energy. For Lindbladian dynamics we use $\Gamma = 0.01|J|$, while for non-Markovian dynamics we use stronger coupling $\Gamma = 0.1|J|$, and the cutoff frequency is chosen as $\omega_m = 3|J|$. Note that choosing too large ω_m brings entanglement of LS to zero on a very short timescale. The initial condition for FI is unentangled pure state $\hat{\rho}(0) = |\Sigma\rangle\langle\Sigma|$, where $|\Sigma\rangle = |\rightarrow\rightarrow\rightarrow\rightarrow\rangle$ with all spins pointing along the x-axis. The magnetic field applied for $t \geq 0$, $g\mu_B B_z = 0.8|J|$, is along the z-axis. The initial condition for AFI is unentangled pure state $\hat{\rho}(0) = |\Omega\rangle\langle\Omega|$, where $|\Omega\rangle = |\sigma_1\sigma_2\sigma_1\sigma_2\rangle$ with $\langle\sigma_{1(2)}|\hat{\mathbf{S}}_{1(2)}|\sigma_{1(2)}\rangle$ pointing along $\theta_1 = 1/8$ or $\theta_2 = \pi - 1/8$ and $\phi_{1(2)} = 0$ in spherical coordinates.

In the course of time evolution, $\hat{\rho}(t)$ can become entangled which is quantified by computing entanglement negativity [12–16] between the left half (LH) and the right half (RH) of the chain $E_N[\hat{\rho}(t)] = \ln||\hat{\rho}^{T_{\rm RH}}||_1 = \ln\sum_n |\lambda_n|$, where $||\hat{A}||_1 = {\rm Tr}\sqrt{\hat{A}^\dagger\hat{A}}$ is the trace norm of the operator $\hat{A}$; λ_n are the eigenvalues of $\hat{\rho}^{T_{\rm RH}}$; and the matrix elements of the partial transpose with respect to RH of the chain are given by $\left(\hat{\rho}^{T_{\rm RH}}\right)_{i\alpha;j\beta} = \left(\hat{\rho}\right)_{j\alpha;i\beta}$. While the standard von Neunmann entanglement entropy $\mathcal{S}_{\rm LH}$ of half of the chain [7, 18] can be non-zero even for unentangled mixed state in Eq. (1), non-zero E_N necessarily implies entanglement and genuine quantum correlations between the two parts [12–16].

Initially, both FI and AFI exhibit dynamical build-up of entanglement signified by $E_N > 0$ in Figs. 1 and 2, respectively. However, Lindbladian dynamics quickly brings $E_N \to 0$ in the FI hosting $S = 1/2$ [Fig. 1(e)], $S = 1$ (Fig. S1(g) in the SM [77]), and $S = 5/2$ [Fig. 1(g)] spins; as well as in the AFI hosting $S = 5/2$ [Fig. 2(e)] spins. Establishing $E_N \to 0$ also makes it possible for LLG classical trajectories $\mathbf{S}_i(t)$ to track $\langle\hat{\mathbf{S}}_i\rangle(t)$ in Figs. 1, 2 and S1 in the SM [77]. Details of how the LLG equation is solved to obtain $\mathbf{S}_i(t)$, while tuning the Gilbert damping parameter in order to enable comparison of $\mathbf{S}_i(t)$ and $\langle\hat{\mathbf{S}}_i\rangle(t)$, are given in the SM [77]. In the AFI case with $S = 1/2$ [Fig. 2(e)] or $S = 1$ (Fig. S1(c) in the SM [77]) entanglement *never* vanishes, $E_N(t) > 0$, even in the long-time limit, thereby maintaining $\langle\hat{\mathbf{S}}_i\rangle(t) \neq \mathbf{S}_i(t)$. Thus, we conclude that usage [36–39, 43] of the LLG equation in spintronics with AFI layers hosting spins $S = 1/2$ or $S = 1$ *cannot be justified microscopically.* In the case of non-Markovian dynamics, $E_N(t)$ remains non-zero (Figs. 1, 2 and S1 in the SM[77]) in FI and AFI at all times and for $S = 1/2$, $S = 1$ and $S = 5/2$, so that quantum-to-classical transition $\langle\hat{\mathbf{S}}_i\rangle(t) \mapsto \mathbf{S}_i(t)$ is *never* achieved. This then provides an example of how pronounced memory effects can lead to revival of genuine quantum properties such as quantum coherence, correlations, and entanglement [63].

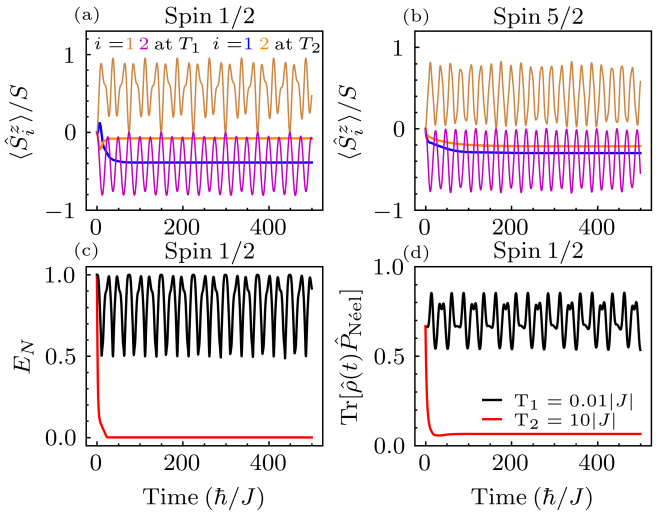

FIG. 3. Time dependence of: (a),(b) spin expectation values at sites $i = 1, 2$; (c) entanglement negativity $E_N(t)$ [12] between two halves of AFI chain; and (d) overlap between the chain density matrix $\hat{\rho}(t)$ and pure states in the Néel subspace. The AFI chain has $N = 4$ sites, as well as an impurity introducing the z-axis anisotropy at site $i = 1$ [Eq. (8)]. The Lindblad Eq. (3) evolves $\hat{\rho}(t)$ upon coupling AFI chain to the bosonic bath at $t = 0$, starting from pure entangled GS but exhibiting Néel "checkerboard" order $\langle \hat{S}_i^z \rangle = -\langle \hat{S}_{i+1}^z \rangle \neq 0$ [26].

Finally, we examine the fate of entangled GS of AFI upon *suddenly coupling* it to a bosonic bath and evolving it by the Lindblad Eq. (3). Let us recall that a common trick employed in TN calculations on spin systems to select the unentangled Néel state as the GS is to introduce an external staggered magnetic field which alternates in sign on atomic length scales [78]. However, its microscopic justification is missing. Attempts to introduce more realistic decoherence mechanisms, such as repeated local measurements [79–81] that would disrupt superposition in the GS and replace the need for contrived staggered field, are also difficult to justify in the context of spintronic and magnonic devices. A handful of recent studies have examined time evolution of entangled GS of AFIs [67, 82] upon suddenly coupling their spins to a dissipative environment, but with conflicting conclusions about the fate of entanglement. Since the "checkerboard" pattern of expectation values of $\langle \hat{\mathbf{S}}_i \rangle$ in the Néel order is often reported experimentally [40], we induce it as the initial condition at $t = 0$ by using GS of slightly modified Heisenberg Hamiltonian

$$\hat{H}_{\text{imp}} = \hat{H}_H - 0.2|J|\hat{S}_1^z, \tag{8}$$

with an additional impurity at site $i = 1$. The impurity breaks rotational invariance of $\hat{H}_H$ to generate Néel order, $\langle \hat{S}_i^z \rangle = -\langle \hat{S}_{i+1}^z \rangle \neq 0$, *but not* the Néel GS $|\uparrow\downarrow\uparrow\downarrow\rangle$ because entanglement entropy of true GS remains nonzero [26] leading to $\langle \hat{S}_i^z \rangle / S < 1$. The Lindbladian time evolution [Fig. 3] maintains entanglement $E_N(t) > 0$ at low temperature $T_1 = 0.01|J|$ and, therefore, *non-classical* dynamics of $\langle \hat{\mathbf{S}}_i \rangle(t)$, while at high temperatures $E_N \to 0$ is reached on short time scales. The overlap $\mathrm{Tr}\,[\hat{\rho}(t)\hat{P}_{\text{Néel}}]$ with states in the Néel subspace, whose projector is $\hat{P}_{\text{Néel}} = |\uparrow\downarrow\uparrow\downarrow\rangle\langle\uparrow\downarrow\uparrow\downarrow| + |\downarrow\uparrow\downarrow\uparrow\rangle\langle\downarrow\uparrow\downarrow\uparrow|$, never reaches 1 in the low temperature regime [black curve in Fig. 3(d)]. In the high temperature limit, the overlap becomes negligible [red curve in Fig. 3(d)] as the system goes [82] into *static ferrimagnetic* ordering [blue and orange flat lines in Figs. 3(a) and 3(b)].

In conclusion, we solve nearly a century old [49] problem—"unreasonable effectiveness" of the classical LLG equation in describing dynamics of *many* (for solution of the same problem for a single spin, see Ref. [58]) localized spins within a magnetic material—by showing that it is justified microscopically only if Lindblad open quantum system dynamics is generated by environment in the case of any ferromagnet, as well as for antiferromagnets with sufficiently large value of their spin $S > 1$. *Thus, our findings exclude antiferromagnets with $S = 1/2$ or $S = 1$ spins from possibility to model them via classical micromagnetics or ASD* [59, 60]. Our analysis via rigorously constructed Markovian and non-Markovian QMEs for many LS interacting with bosonic bath could also be applied to other related problems, such as fate of entanglement in quantum spin liquids [83].

This research was primarily supported by the US National Science Foundation through the University of Delaware Materials Research Science and Engineering Center, DMR-2011824.

* bnikolic@udel.edu

[1] N. B. Christensen, H. M. Rønnow, D. F. McMorrow, A. Harrison, T. G. Perring, M. Enderle, R. Coldea, L. P. Regnault, and G. Aeppli, Quantum dynamics and entanglement of spins on a square lattice, PNAS **104**, 15264 (2007).

[2] T. Brydges, A. Elben, P. Jurcevic, B. Vermersch, C. Maier, B. Lanyon, P. Zoller, R. Blatt, and C. Roos, Probing Rényi entanglement entropy via randomized measurements, Science **364**, 260 (2019).

[3] A. Scheie, P. Laurell, A. M. Samarakoon, B. Lake, S. E. Nagler, G. E. Granroth, S. Okamoto, G. Alvarez, and D. A. Tennant, Witnessing entanglement in quantum magnets using neutron scattering, Phys. Rev. B **103**, 224434 (2021).

[4] G. Mathew, S. L. L. Silva, A. Jain, A. Mohan, D. T. Adroja, V. G. Sakai, C. V. Tomy, A. Banerjee, R. Goreti, A. V. N., R. Singh, and D. Jaiswal-Nagar, Experimental realization of multipartite entanglement via quantum Fisher information in a uniform antiferromagnetic quantum spin chain, Phys. Rev. Res. **2**, 043329 (2020).

[5] P. Laurell, A. Scheie, C. J. Mukherjee, M. M. Koza, M. Enderle, Z. Tylczynski, S. Okamoto, R. Coldea, D. A. Tennant, and G. Alvarez, Quantifying and

controlling entanglement in the quantum magnet Cs_2CoCl_4, Phys. Rev. Lett. **127**, 037201 (2021).
[6] N. Friis, G. Vitagliano, M. Malik, and M. Huber, Entanglement certification from theory to experiment, Nat. Rev. Phys. **1**, 72 (2018).
[7] G. D. Chiara and A. Sanpera, Genuine quantum correlations in quantum many-body systems: a review of recent progress, Rep. Prog. Phys. **81**, 074002 (2018).
[8] N. Laflorencie, Quantum entanglement in condensed matter systems, Phys. Rep. **646**, 1 (2016).
[9] H. F. Song, N. Laflorencie, S. Rachel, and K. Le Hur, Entanglement entropy of the two-dimensional Heisenberg antiferromagnet, Phys. Rev. B **83**, 224410 (2011).
[10] J. Hales, U. Bajpai, T. Liu, D. R. Baykusheva, M. Li, M. Mitrano, and Y. Wang, Witnessing light-driven entanglement using time-resolved resonant inelastic X-ray scattering, Nat. Commun. **14**, 3512 (2023).
[11] D. R. Baykusheva, M. H. Kalthoff, D. Hofmann, M. Claassen, D. M. Kennes, M. A. Sentef, and M. Mitrano, Witnessing nonequilibrium entanglement dynamics in a strongly correlated fermionic chain, Phys. Rev. Lett. **130**, 106902 (2023).
[12] A. Peres, Separability criterion for density matrices, Phys. Rev. Lett. **77**, 1413 (1996).
[13] K.-H. Wu, T.-C. Lu, C.-M. Chung, Y.-J. Kao, and T. Grover, Entanglement Renyi negativity across a finite temperature transition: A Monte Carlo study, Phys. Rev. Lett. **125**, 140603 (2020).
[14] A. Elben, R. Kueng, H.-Y. Huang, R. van Bijnen, C. Kokail, M. Dalmonte, P. Calabrese, B. Kraus, J. Preskill, P. Zoller, and B. Vermersch, Mixed-state entanglement from local randomized measurements, Phys. Rev. Lett. **125**, 200501 (2020).
[15] S. Sang, Y. Li, T. Zhou, X. Chen, T. H. Hsieh, and M. P. Fisher, Entanglement negativity at measurement-induced criticality, PRX Quantum **2**, 030313 (2021).
[16] L. Aolita, F. de Melo, and L. Davidovich, Open-system dynamics of entanglement:a key issues review, Rep. Prog. Phys. **78**, 042001 (2015).
[17] M. C. Bañuls, Tensor network algorithms: A route map, Annu. Rev. Condens. Matter Phys. **14**, 173 (2023).
[18] J. H. Bardarson, F. Pollmann, and J. E. Moore, Unbounded growth of entanglement in models of many-body localization, Phys. Rev. Lett. **109**, 017202 (2012).
[19] R. Trivedi and J. I. Cirac, Transitions in computational complexity of continuous-time local open quantum dynamics, Phys. Rev. Lett. **129**, 260405 (2022).
[20] A. Lerose, M. Sonner, and D. A. Abanin, Overcoming the entanglement barrier in quantum many-body dynamics via space-time duality, Phys. Rev. B **107**, L060305 (2023).
[21] S. Sahling, G. Remenyi, C. Paulsen, P. Monceau, V. Saligrama, C. Marin, A. Revcolevschi, L. P. Regnault, S. Raymond, and J. E. Lorenzo, Experimental realization of long-distance entanglement between spins in antiferromagnetic quantum spin chains, Nat. Phys. **11**, 255 (2015).
[22] F. H. L. Essler, H. Frahm, F. Göhmann, A. Klümper, and V. E. Korepin, *The One-Dimensional Hubbard Model* (Cambridge University Press, 2005).
[23] A. Singh and Z. Tešanović, Quantum spin fluctuations in an itinerant antiferromagnet, Phys. Rev. B **41**, 11457 (1990).
[24] R. Wieser, Description of a dissipative quantum spin dynamics with a Landau-Lifshitz/Gilbert like damping and complete derivation of the classical Landau-Lifshitz equation, Eur. Phys. J. B **88**, 77 (2015).
[25] P. Mondal, A. Suresh, and B. K. Nikolić, When can localized spins interacting with conduction electrons in ferro- or antiferromagnets be described classically via the Landau-Lifshitz equation: Transition from quantum many-body entangled to quantum-classical nonequilibrium states, Phys. Rev. B **104**, 214401 (2021).
[26] M. D. Petrović, P. Mondal, A. E. Feiguin, and B. K. Nikolić, Quantum spin torque driven transmutation of an antiferromagnetic Mott insulator, Phys. Rev. Lett. **126**, 197202 (2021).
[27] J. S. Pratt, Universality in the entanglement structure of ferromagnets, Phys. Rev. Lett. **93**, 237205 (2004).
[28] U. Bajpai, A. Suresh, and B. K. Nikolić, Quantum many-body states and Green's functions of nonequilibrium electron-magnon systems: Localized spin operators versus their mapping to Holstein-Primakoff bosons, Phys. Rev. B **104**, 184425 (2021).
[29] H. Yuan, Y. Cao, A. Kamra, R. A. Duine, and P. Yan, Quantum magnonics: When magnon spintronics meets quantum information science, Phys. Rep. **965**, 1 (2022).
[30] T. Morimae, A. Sugita, and A. Shimizu, Macroscopic entanglement of many-magnon states, Phys. Rev. A **71**, 032317 (2005).
[31] D. Lachance-Quirion, S. P. Wolski, Y. Tabuchi, S. Kono, K. Usami, and Y. Nakamura, Entanglement-based single-shot detection of a single magnon with a superconducting qubit, Science **367**, 425 (2020).
[32] J. S. Pratt, Qubit entanglement in multimagnon states, Phys. Rev. B **73**, 184413 (2006).
[33] A. R. R. Carvalho, F. Mintert, and A. Buchleitner, Decoherence and multipartite entanglement, Phys. Rev. Lett. **93**, 230501 (2004).
[34] H. Y. Yuan, W. P. Sterk, A. Kamra, and R. A. Duine, Master equation approach to magnon relaxation and dephasing, Phys. Rev. B **106**, 224422 (2022).
[35] H. Y. Yuan, W. P. Sterk, A. Kamra, and R. A. Duine, Pure dephasing of magnonic quantum states, Phys. Rev. B **106**, L100403 (2022).
[36] V. Baltz, A. Manchon, M. Tsoi, T. Moriyama, T. Ono, and Y. Tserkovnyak, Antiferromagnetic spintronics, Rev. Mod. Phys. **90**, 015005 (2018).
[37] T. Jungwirth, X. Marti, P. Wadley, and J. Wunderlich, Antiferromagnetic spintronics, Nat. Nanotechnol **11**, 231 (2016).
[38] J. Zelezny, P. Wadley, K. Olejnik, A. Hoffmann, and H. Ohno, Spin transport and spin torque in antiferromagnetic devices, Nat. Phys. **14**, 220–228 (2018).
[39] M. B. Jungfleisch, W. Zhang, and A. Hoffmann, Perspectives of antiferromagnetic spintronics, Phys. Lett. A **382**, 865 (2018).
[40] I. Gray, T. Moriyama, N. Sivadas, G. M. Stiehl, J. T. Heron, R. Need, B. J. Kirby, D. H. Low, K. C. Nowack, D. G. Schlom, D. C. Ralph, T. Ono, and G. D. Fuchs, Spin Seebeck imaging of spin-torque switching in antiferromagnetic Pt/NiO heterostructures, Phys. Rev. X **9**, 041016 (2019).
[41] U. Ritzmann, P. Baláž, P. Maldonado, K. Carva, and P. M. Oppeneer, High-frequency magnon excitation due to femtosecond spin-transfer torques, Phys. Rev. B **101**, 174427 (2020).
[42] A. Suresh, U. Bajpai, M. D. Petrović, H. Yang, and

B. K. Nikolić, Magnon- versus electron-mediated spin-transfer torque exerted by spin current across an antiferromagnetic insulator to switch the magnetization of an adjacent ferromagnetic metal, Phys. Rev. Applied **15**, 034089 (2021).
[43] R. Cheng, J. Xiao, Q. Niu, and A. Brataas, Spin pumping and spin-transfer torques in antiferromagnets, Phys. Rev. Lett. **113**, 057601 (2014).
[44] Y. Wang, D. Zhu, Y. Yang, K. Lee, R. Mishra, G. Go, S.-H. Oh, D.-H. Kim, K. Cai, E. Liu, S. D. Pollard, S. Shi, J. Lee, K. L. Teo, Y. Wu, K.-J. Lee, and H. Yang, Magnetization switching by magnon-mediated spin torque through an antiferromagnetic insulator, Science **366**, 1125 (2019).
[45] P. Vaidya, S. A. Morley, J. van Tol, Y. Liu, R. Cheng, A. Brataas, D. Lederman, and E. del Barco, Subterahertz spin pumping from an insulating antiferromagnet, Science **368**, 160 (2020).
[46] J. Li, C. Wilson, R. Cheng, M. Lohmann, M. Kavand, W. Yuan, M. Aldosary, N. Agladze, P. Wei, M. Sherwin, and J. Shi, Spin current from sub-terahertz-generated antiferromagnetic magnons, Nature **578**, 1 (2020).
[47] H. Qiu, L. Zhou, C. Zhang, J. Wu, Y. Tian, S. Cheng, S. Mi, H. Zhao, Q. Zhang, D. Wu, B. Jin, J. Chen, and P. Wu, Ultrafast spin current generated from an antiferromagnet, Nat. Phys. **17**, 1 (2021).
[48] H. Y. Yuan, Q. Liu, K. Xia, Z. Yuan, and X. R. Wang, Proper dissipative torques in antiferromagnetic dynamics, EPL **126**, 67006 (2019).
[49] L. D. Landau and E. M. Lifshitz, On the theory of the dispersion of magnetic permeability in ferromagnetic bodies, Phys. Z. Sowjetunion **8**, 153 (1935).
[50] T. Gilbert, A phenomenological theory of damping in ferromagnetic materials, IEEE Trans. Magn. **40**, 3443 (2004).
[51] W. M. Saslow, Landau–Lifshitz or Gilbert damping? that is the question, J. Appl. Phys. **105**, 07D315 (2009).
[52] J. Gauyacq and N. Lorente, Classical limit of a quantal nano-magnet in an anisotropic environment, Surf. Sci. **630**, 325 (2014).
[53] J. L. García-Palacios and D. Zueco, Solving spin quantum master equations with matrix continued-fraction methods: application to superparamagnets, J. Phys. A: Math. Theor. **39**, 13243 (2006).
[54] R. Wieser, Comparison of quantum and classical relaxation in spin dynamics, Phys. Rev. Lett. **110**, 147201 (2013).
[55] J. B. Parkinson, J. C. Bonner, G. Müller, M. P. Nightingale, and H. W. J. Blöte, Heisenberg spin chains: Quantum-classical crossover and the haldane conjecture, J. Appl. Phys. **57**, 3319 (1985).
[56] E. Kaxiras and J. D. Joannopoulos, *Quantum theory of materials* (Cambridge University Press, 2019).
[57] A. J. Leggett, S. Chakravarty, A. T. Dorsey, M. P. A. Fisher, A. Garg, and W. Zwerger, Dynamics of the dissipative two-state system, Rev. Mod. Phys. **59**, 1 (1987).
[58] J. Anders, C. Sait, and S. Horsley, Quantum Brownian motion for magnets, New J. Phys. **24**, 033020 (2022).
[59] R. F. L. Evans, W. J. Fan, P. Chureemart, T. A. Ostler, M. O. A. Ellis, and R. W. Chantrell, Atomistic spin model simulations of magnetic nanomaterials, J. Phys. Condens. **26**, 103202 (2014).
[60] S.-K. Kim, Micromagnetic computer simulations of spin waves in nanometre-scale patterned magnetic elements, J. Phys. D: Appl. Phys. **43**, 264004 (2010).
[61] M. D. Petrović, P. Mondal, A. E. Feiguin, P. Plecháč, and B. K. Nikolić, Spintronics meets density matrix renormalization group: Quantum spin-torque-driven nonclassical magnetization reversal and dynamical buildup of long-range entanglement, Phys. Rev. X **11**, 021062 (2021).
[62] H.-P. Breuer and F. Petruccione, *The Theory of Open Quantum Systems* (Oxford University PressOxford, 2007).
[63] H.-P. Breuer, E.-M. Laine, J. Piilo, and B. Vacchini, Colloquium: Non-Markovian dynamics in open quantum systems, Rev. Mod. Phys. **88**, 021002 (2016).
[64] I. de Vega and D. Alonso, Dynamics of non-Markovian open quantum systems, Rev. Mod. Phys. **89**, 015001 (2017).
[65] F. Nathan and M. S. Rudner, Universal Lindblad equation for open quantum systems, Phys. Rev. B **102**, 115109 (2020).
[66] G. Schaller, *Open Quantum Systems Far from Equilibrium* (Springer International Publishing, 2014).
[67] M. Weber, D. J. Luitz, and F. F. Assaad, Dissipation-induced order: The $S = 1/2$ quantum spin chain coupled to an Ohmic bath, Phys. Rev. Lett. **129**, 056402 (2022).
[68] D. Manzano, A short introduction to the Lindblad master equation, AIP Adv. **10**, 025106 (2020).
[69] G. Lindblad, On the generators of quantum dynamical semigroups, Commun. Math. Phys. **48**, 119 (1976).
[70] A. Norambuena, A. Franco, and R. Coto, From the open generalized Heisenberg model to the Landau–Lifshitz equation, New J. Phys. **22**, 103029 (2020).
[71] G. B. Cuetara, M. Esposito, and G. Schaller, Quantum thermodynamics with degenerate eigenstate coherences, Entropy **18**, 447 (2016).
[72] E. Mozgunov and D. Lidar, Completely positive master equation for arbitrary driving and small level spacing, Quantum **4**, 227 (2020).
[73] G. McCauley, B. Cruikshank, D. I. Bondar, and K. Jacobs, Accurate Lindblad-form master equation for weakly damped quantum systems across all regimes, Npj Quantum Inf. **6**, 74 (2020).
[74] G. T. Landi, D. Poletti, and G. Schaller, Nonequilibrium boundary-driven quantum systems: Models, methods, and properties, Rev. Mod. Phys. **94**, 045006 (2022).
[75] A. Nazir and G. Schaller, The reaction coordinate mapping in quantum thermodynamics, in *Thermodynamics in the Quantum Regime: Fundamental Aspects and New Directions*, edited by F. Binder, L. A. Correa, C. Gogolin, J. Anders, and G. Adesso (Springer, Cham, 2018) pp. 551–577.
[76] N. Anto-Sztrikacs and D. Segal, Strong coupling effects in quantum thermal transport with the reaction coordinate method, New J. Phys. **23**, 063036 (2021).
[77] See Supplemental Material at https://wiki.physics.udel.edu/qttg/Publications, which includes Refs.[84–100], for: additional Fig. S1 as the counterpart of Figs. 1 and 2, but considering $S = 1$ LS within either FI or AFI chains; numerical procedures for solving the LLG equation for $\mathbf{S}_i(t)$, as well as for comparing $\mathbf{S}_i(t)$ with $\langle\hat{\mathbf{S}}_i\rangle(t)$ which also allows one to extract *microscopcially* the Gilbert damping in the LLG equation; the effect of additional interactions acting on

LS, such as easy-axis anisotropy, dipole-dipole interaction and Dzyaloshinskii–Moriya interaction; usage of a single vs. many independent bosonic baths; exploration of wide range of temperatures of bosonic baths; proximity of steady-state solution of the Lindblad QME to Gibbs density matrix describing thermal equilibrium; and scaling of entanglement with increasing number of spins.

[78] E. Stoudenmire and S. R. White, Studying two-dimensional systems with the density matrix renormalization group, Annu. Rev. Condens. Matter Phys. **3**, 111 (2012).

[79] M. I. Katsnelson, V. V. Dobrovitski, and B. N. Harmon, Néel state of an antiferromagnet as a result of a local measurement in the distributed quantum system, Phys. Rev. B **63**, 212404 (2001).

[80] H. C. Donker, H. De Raedt, and M. I. Katsnelson, Decoherence wave in magnetic systems and creation of Néel antiferromagnetic state by measurement, Phys. Rev. B **93**, 184426 (2016).

[81] H. C. Donker, H. De Raedt, and M. I. Katsnelson, Antiferromagnetic order without recourse to staggered fields, Phys. Rev. B **98**, 014416 (2018).

[82] G. Schaller, F. Queisser, N. Szpak, J. König, and R. Schützhold, Environment-induced decay dynamics of antiferromagnetic order in Mott-Hubbard systems, Phys. Rev. B **105**, 115139 (2022).

[83] K. Yang, S. C. Morampudi, and E. J. Bergholtz, Exceptional spin liquids from couplings to the environment, Phys. Rev. Lett. **126**, 077201 (2021).

[84] A. Szilva, Y. Kvashnin, E. A. Stepanov, L. Nordström, O. Eriksson, A. I. Lichtenstein, and M. I. Katsnelson, Quantitative theory of magnetic interactions in solids, Rev. Mod. Phys. **95**, 035004 (2023).

[85] R. P. Erickson, Long-range dipole-dipole interactions in a two-dimensional Heisenberg ferromagnet, Phys. Rev. B **46**, 14194 (1992).

[86] M. Sharma, Govind, A. Pratap, Ajay, and R. Tripathi, Role of dipole-dipole interaction on the magnetic dynamics of anisotropic layered cuprate antiferromagnets, Phys. Stat. Sol. B **226**, 193 (2001).

[87] E. Davis, B. Ye, F. Machado, S. Meynell, W. Wu, T. Mittiga, W. Schenken, M. Joos, B. Kobrin, Y. Lyu, Z. Wang, D. Bluvstein, S. Choi, C. Zu, A. Jayich, and N. Yao, Probing many-body dynamics in a two-dimensional dipolar spin ensemble, Nat. Phys. **19**, 836 (2023).

[88] B. Sbierski, M. Bintz, S. Chatterjee, M. Schuler, N. Y. Yao, and L. Pollet, Magnetism in the two-dimensional dipolar XY model, arXiv:2305.03673 (2023).

[89] R. E. Camley and K. L. Livesey, Consequences of the Dzyaloshinskii-Moriya interaction, Surf. Sci. Rep. **78**, 100605 (2023).

[90] T. Prosen, Exact nonequilibrium steady state of an open Hubbard chain, Phys. Rev. Lett. **112**, 030603 (2014).

[91] F. Queisser and R. Schützhold, Environment-induced prerelaxation in the Mott-Hubbard model, Phys. Rev. B **99**, 155110 (2019).

[92] J. S. Lee and J. Yeo, Comment on "Universal Lindblad equation for open quantum systems", arXiv:2011.00735 (2020).

[93] F. Nathan and M. S. Rudner, High accuracy steady states obtained from the universal Lindblad equation, arXiv:2206.02917 (2022).

[94] J. L. García-Palacios and F. J. Lázaro, Langevin-dynamics study of the dynamical properties of small magnetic particles, Phys. Rev. B **58**, 14937 (1998).

[95] J. Zou, S. K. Kim, and Y. Tserkovnyak, Tuning entanglement by squeezing magnons in anisotropic magnets, Phys. Rev. B **101**, 014416 (2020).

[96] F. Iemini, D. Chang, and J. Marino, Dynamics of inhomogeneous spin ensembles with all-to-all interactions: breaking permutational invariance, arXiv:2309.10746 (2023).

[97] A. Seif, Y.-X. Wang, and A. A. Clerk, Distinguishing between quantum and classical Markovian dephasing dissipation, Phys. Rev. Lett. **128**, 070402 (2022).

[98] M. A. Nielsen and I. L. Chuang, *Quantum Computation and Quantum Information: 10th Anniversary Edition* (Cambridge University Press, 2010).

[99] J. D. Cresser and J. Anders, Weak and ultrastrong coupling limits of the quantum mean force Gibbs state, Phys. Rev. Lett. **127**, 250601 (2021).

[100] A. Schuckert, A. Orioli, and J. Berges, Nonequilibrium quantum spin dynamics from two-particle irreducible functional integral techniques in the Schwinger boson representation, Phys. Rev. B **98**, 224304 (2018).

Supplemental Material for "Fate of entanglement in magnetism under Lindbladian or non-Markovian dynamics and conditions for their transition to Landau-Lifshitz-Gilbert classical dynamics"

Federico Garcia-Gaitan and Branislav K. Nikolić*
Department of Physics and Astronomy, University of Delaware, Newark, DE 19716, USA

This Supplemental Material provides *eight* additional Figs. S1–Fig. S8, as well as details of how the Landau-Lifshitz-Gilbert (LLG) [1–3] equation is solved in order to obtain classical trajectories $\mathbf{S}_i(t)$ of localized spins. We also explain how to properly compare $\mathbf{S}_i(t)$ with time-evolution of quantum expectation values of localized spins $\langle\hat{\mathbf{S}}_i\rangle(t)$ while microscopically extracting in this process the Gilbert damping parameter from open quantum system dynamics. Additional Figures S1–Fig. S8 cover cases of: different types of interactions (not studied in the main text) acting on localized spins, such as easy-axis anisotropy [2, 4], dipole-dipole interaction [5–8] and Dzyaloshinskii–Moriya interaction (DMI) [4, 9]; usage of a single global vs. many local independent (as employed in the main text, as well as in other studies [10–14]) bosonic baths coupled to localized spins; exploration of wide range of temperatures of bosonic baths; proximity [15, 16] of steady-state solution of the universal [10] Lindblad quantum master equation (QME) in our problem to Gibbs density matrix describing thermal equilibrium; and scaling of entanglement with increasing number of localizes spins in order to confirm that our conclusions are largely independent of the system size. In all Figures S1–S8, the nonequilibrium dynamics of spin chains modeling antiferromagnetic insulator (AFI) or ferromagnetic insulator (FI), and viewed as open quantum systems [17–19], is initiated in the same way as explained in the main text.

I. FERRO- OR ANTIFERROMAGNETIC INSULATOR HOSTING LOCALIZED SPINS $S = 1$

Figure S1 is the *counterpart* of Figs. 1 and 2 in the main text, but considering $S = 1$ localized spins hosted by AFI [Fig. S1(a)–(d)] or FI [Fig. S1(e)–(h)].

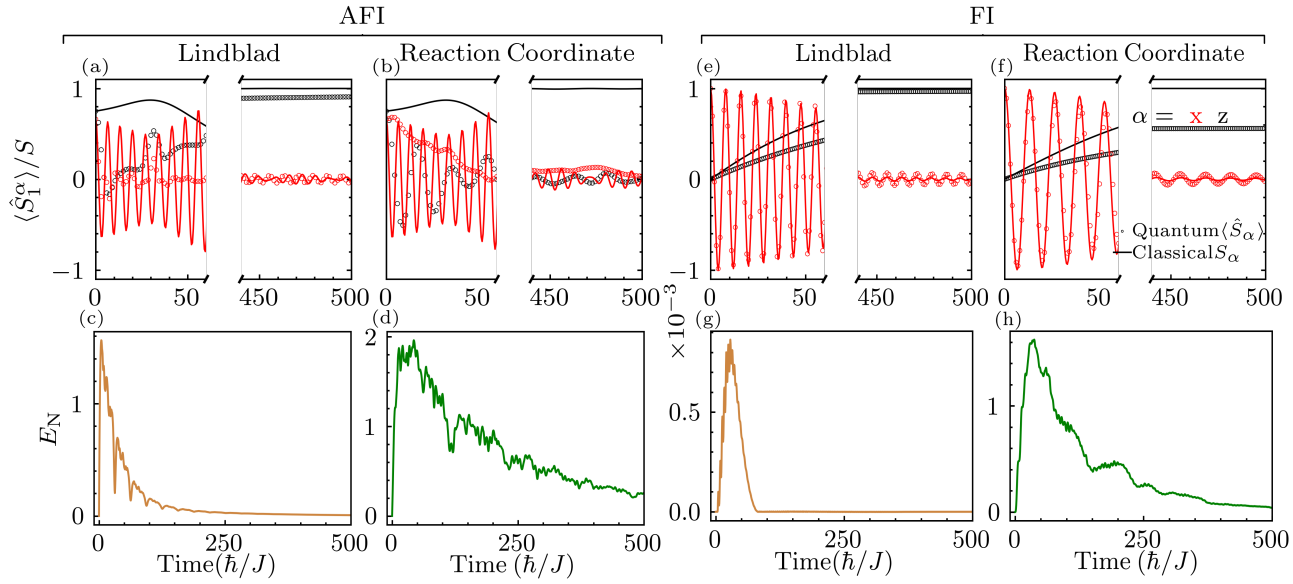

FIG. S1. Time-dependence of QME-computed $\langle\hat{S}_1^\alpha\rangle(t)$ vs. classical-LLG-computed $S_1^\alpha(t)$ of LS $S = 1$ on site $i = 1$ of (a),(b) AFI chain and (e),(f) FI chain. Time dependence of entanglement negativity $E_N(t)$ measuring entanglement between two halves of (c),(d) AFI chain or (g),(h) FI chain in the case of quantum dynamics (circles) in panels (a),(b) or (e),(f), respectively. The localized spins within FI or AFI are evoloved as an open quantum system [17–19] using either Lindblad (i.e., Markovian) or RC (i.e., non-Markovian) QME with bosonic bath temperature $T = |J|$, as discussed in details in the main text.

* bnikolic@udel.edu

II. SOLVING STOCHASTIC LANDAU-LIFSHITZ-GILBERT EQUATION AND EXTRACTING ITS DAMPING MICROSCOPICALLY FROM OPEN QUANTUM SYSTEM DYNAMICS

The classical dynamics of localized spins $\mathbf{S}_i$ is computed by the phenomenological LLG equation [1–3]

$$\frac{\partial \mathbf{S}_i}{\partial t} = -g\mathbf{S}_i \times (\mathbf{B}_i^{\text{eff}} + \mathbf{B}_i^{\text{th}}) + \lambda \mathbf{S}_i \times \frac{\partial \mathbf{S}_i}{\partial t}. \tag{1}$$

extended into its stochastic version [20] by the usage of a thermal magnetic field $\mathbf{B}_i^{\text{th}}(t)$ as random variable. Here λ is the Gilbert damping parameter [3], in the context of atomistic spin dynamics [2] where each atom of the lattice hosts one vector $\mathbf{S}_i$; g is the gyromagnetic ratio; and

$$\mathbf{B}_i^{\text{eff}} = -\frac{1}{\mu_M}\frac{\partial \mathcal{H}}{\partial \mathbf{S}_i}, \tag{2}$$

is the effective magnetic field obtained from the classical Heisenberg Hamiltonian,

$$\mathcal{H} = J\sum_{\langle ij \rangle} \mathbf{S}_i \cdot \mathbf{S}_j - \sum_i g\mu_B \mathbf{B}_{\text{ext}}(t \geq 0) \cdot \mathbf{S}_i, \tag{3}$$

with μ_M being the magnitude of classical localized spins [2] and μ_B is the Bohr magneton. The thermal fluctuations of classical localized spins $\mathbf{S}_i(t)$ are represented by a stochastic Langevin process, where their Brownian motion is simulated using $\mathbf{B}_i^{\text{th}}(t)$ as a Gaussian random variable [20] with zero mean in all Cartesian components, $\overline{\mathrm{B}_i^{\text{th},\alpha}(t)} = 0$, and correlator $\overline{\mathrm{B}_i^{\text{th},\alpha}(t)\mathrm{B}_i^{\text{th},\beta}(t')} = 2D\delta_{\alpha,\beta}\delta(t-t')$, where $D = \frac{\lambda}{1+\lambda^2}k_B T$.

The LLG equation is solved using time step $\delta t = 0.01\hbar/J$ within the stochastic generalization of the Heun method [2], which is equivalent to the second order Runge-Kutta method and includes the stochastic nature $\mathbf{B}_i^{\text{th}}(t)$ [20]. For all cases, we average over 100 independent simulations. The Gilbert damping parameter is obtained by minimizing the root-mean-square of the difference between quantum and classical trajectories of localized spins when the latter is computed using $\lambda = 0$. Thus, *such a procedure effectively and microscopically extracts the Gilbert damping parameter from open quantum system dynamics*, yielding as the typical value $\lambda = 0.02$. This value, which is often encountered in realistic magnetic materials [2], is then employed in Figs. 1–3 of the main text and in Fig. S1.

III. ROLE OF MAGNETIC ANISOTROPY, LONG-RANGED DIPOLE-DIPOLE AND DZYALOSHINSKII-MORIYA INTERACTIONS

Commonly used effective spin Hamiltonians [2, 4] of bulk magnetic materials and their heterostructures often involve interactions affecting localized spins that are additional to the Heisenberg exchange J (as the only considered one in the main text). Examples of additional interactions are the easy-axis anisotropy [2, 4], dipole-dipole interactions [5–8], and DMI [4, 9]. For example, it has been recently predicted [21] that distant localized spins within an anisotropic FI can become entangled in the presence of magnons, with the amount of entanglement controlled by the external fields and anisotropies. On the other hand, in spintronics [2] and magnonics [22], dynamics of localized spins for respective extended [when compared to plain Heisenberg Hamiltonian in Eq. (3)] models is typically computed by using a straightforward generalization of $\mathbf{B}_i^{\text{eff}}$ in Eq. (2) and, therefore, tacitly assuming that many-spin entanglement studied in the main text has somehow being brought to zero. To properly justify usage of classical LLG dynamics for such extended models requires repeating calculations from the main text—of entanglement negativity $E_N(t)$ which must vanish to enable quantum-to-classical transition $\langle \hat{\mathbf{S}}_i \rangle(t) \mapsto \mathbf{S}_i(t)$—in the presence of these additional interactions.

As discussed in the main text, *the presence of any genuine quantum property—such as quantum coherence, correlations, and entanglement—automatically makes the classical LLG equation inapplicable.* Since in the main text we find that LLG equation can *never* mimic underlying quantum dynamics that is non-Markovian, precisely because its pronounced memory effects can lead to revival [18] of genuine quantum properties including always present nonzero entanglement, we limit our analysis in this Section to localized spins that are weakly [10] coupled to independent bosonic baths and, therefore, describable by Markovian dynamics via the Lindlad QME. That is, we assume that the correlation time of the bath is much shorter than the characteristic timescale of system-bath interactions, while not requiring any restrictions on the internal energy level structure of the system itself, as assumed in the derivation of the universal Lindblad QME [10] we employ here and in the main text.

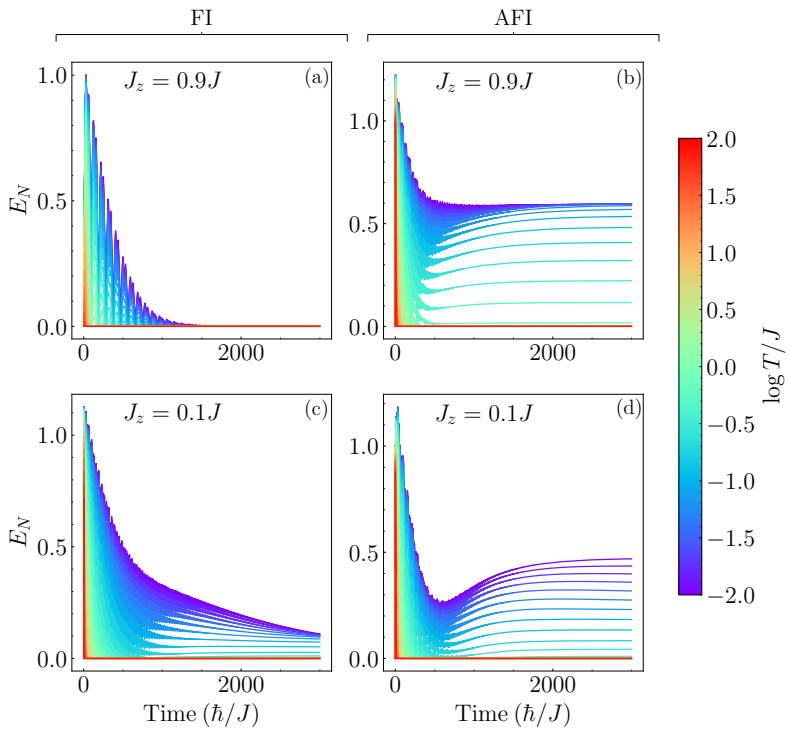

FIG. S2. The Lindblad QME-computed time dependence of entanglement negativity $E_N(t)$ for FI or AFI chain composed of $N = 4$ sites hosting $S = 1/2$ localized spins with periodic boundary conditions and additional [Eq. (4)] easy-axis anisotropy. The color of individual curves denotes different temperatures (color bar on the right) of bosonic baths in the units of Heisenberg exchange coupling J between the localized spins.

A. Easy-axis anisotropy

We first consider an anisotropic Heisenberg Hamiltonian for localized quantum spins $S = 1/2$

$$\hat{H} = \sum_i J(\hat{S}_i^x \hat{S}_{i+1}^x + \hat{S}_i^y \hat{S}_{i+1}^y) + J_z \hat{S}_i^z \hat{S}_{i+1}^z, \tag{4}$$

where $J_z \neq J$ introduces anisotropy. Two different anisotropy values, $J_z = 0.1J$ and $J_z = 0.9J$, are considered for both FI and AFI chain out of equilibrium in Fig. S2. Similarly to the isotropic case considered in Fig. 2 of the main text, the entanglement negativity of AFI [Fig. S2(b) and S2(d)] remains nonzero up to a temperature $T \sim J$. On the other hand, in the FI case [Figs. S2(a) and S2(c)] larger entanglement production is obtained, resulting in nonvanishing entanglement negativity even for temperatures $T \sim 0.6J$ and high anisotropy $J_z = 0.9J$. Nevertheless, one of the principal conclusions of the main text—that the LLG equations is applicable to FIs with arbitrary value of localized spins, as long as they are coupled to Markovian dissipative environment—should hold as anisotropy [4] in realistic magnetic materials is not as large as used in Fig. S2.

B. Long-ranged dipole-dipole interaction

To include long-ranged dipole-dipole interaction between localized quantum spins, we consider a dipolar XY model Hamiltonian as given by [7, 8]

$$\hat{H} = J \sum_{ij} C_{ij}(\hat{S}_i^x \hat{S}_j^x + \hat{S}_i^y \hat{S}_j^y), \tag{5}$$

where $C_{ij} = 1/|\mathbf{r}_i - \mathbf{r}_j|^3$ and $\mathbf{r}_i$ is the position vector of site i. The distance between the nearest-neighbor sites is set to 1, and we consider open boundary conditions. Figure S3 shows the entanglement build-up dynamics for FI and AFI chains. Such entanglement eventually does go to zero, however at low enough temperatures ($T < 0.2J$) the

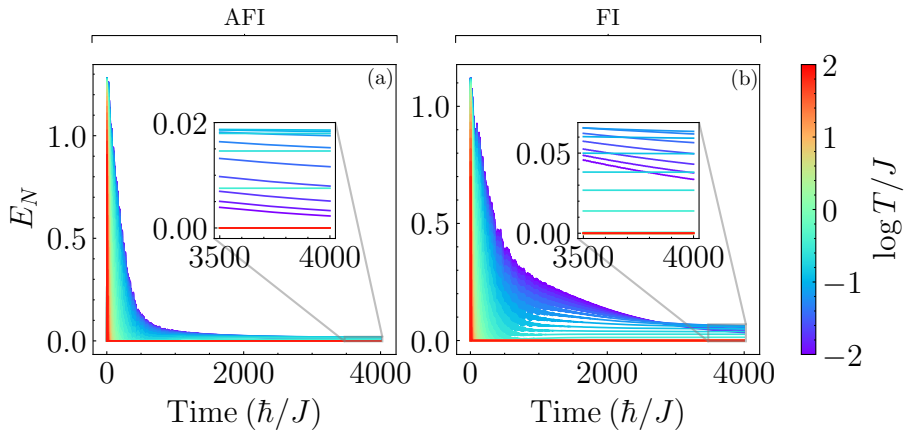

FIG. S3. The Lindblad QME-computed time entanglement negativity $E_N(t)$ for FI or AFI chain composed of $N = 4$ sites hosting spin $S = 1/2$, using periodic boundary conditions and including additional long-ranged dipole-dipole interaction [Eq. (5)]. The color of individual curves denotes different temperatures (color bar on the right) of bosonic baths in the units of Heisenberg exchange coupling J between the localized spins.

decay is notably slower than for the cases without dipole-dipole interaction studied in the main text. This feature can substantially delay quantum-to-classical, therefore also suggesting that quantum corrections should be taken into as also found in very recent experiments on Rydberg atom array realizing a long-range dipolar XY model suggested by previous studies [7, 8]. The existence of distinct decay scales in Lindbladian dynamics has also been reported previously for solid-state platforms [11]. We also recall that dipole-dipole interaction has been discussed for a long time as a mechanism which acts similarly to anisotropy in solid-state magnetic materials in equilibrium, even if real

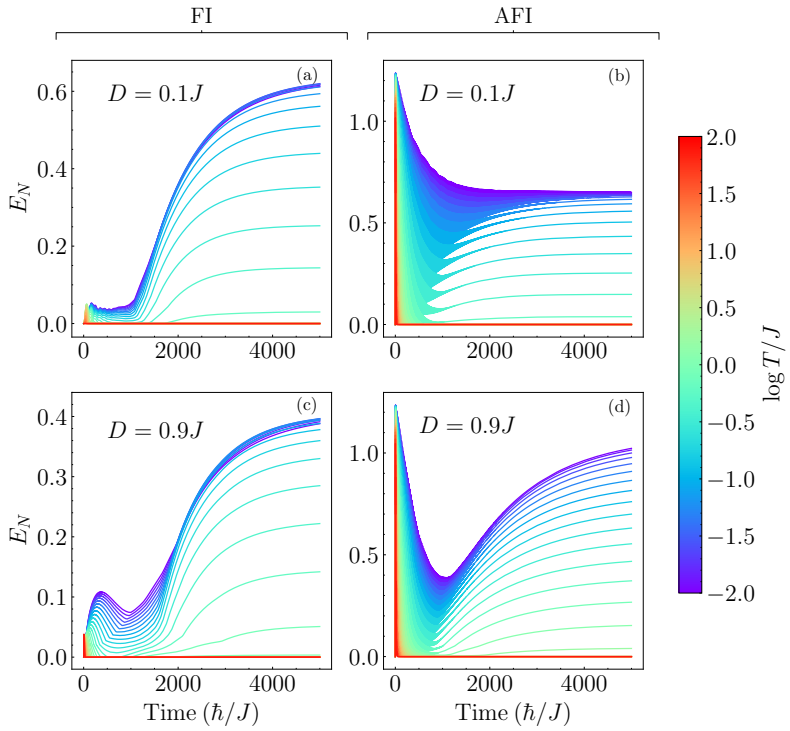

FIG. S4. The Lindblad QME-computed time dependence of logarithmic negativity of a spin-1/2 FI or AFI chain composed of $N = 4$ sites with periodic boundary conditions and additional DMI of strength D (not considered in the main text), see Eq. (S4). The color of individual curves denotes different temperatures (color bar on the right) of bosonic baths in the units of Heisenberg exchange coupling J between the localized spins.

anisotropy [Sec. III A] is absent [5, 6].

C. Dzyaloshinskii-Moriya interaction

Finally, we add DMI into the Heisenberg model, as described by the following quantum Hamiltonian of localized spins

$$\hat{H} = \sum_{\langle ij \rangle} \left[J \hat{\mathbf{S}}_i \cdot \hat{\mathbf{S}}_j + \mathbf{D}_{ij} \cdot (\hat{\mathbf{S}}_i \times \hat{\mathbf{S}}_j) \right], \tag{6}$$

where $\mathbf{D}_{ij} = D\hat{e}_z$ and D measures the strength of DMI [9]. Two different values for D are considered in Fig. S4, $D = 0.1J$ and $D = J$. For $D = 0.1J$ and AFI case, we observe similar dynamics as in the main text or Fig. S1 where entanglement does not vanish, despite Markovian dynamics, due to small value of spin $S = 1/2$. On the other hand, FI case exhibits notably higher entanglement production, leading to nonvanishing entanglement value even in long time limit and at low enough temperatures. Stronger DMI, $D = J$, favor the dynamical entanglement built-up, thus making a transition to LLG classical dynamics *impossible* for temperatures up to $T \sim J$ for *both* FI and AFI. The origin of this new features brought by DMI can be traced to the fact that such interaction favors noncollinearity [9] of spin expectation values, which in systems of interacting quantum spins has been shown to favor entanglement production [23].

IV. USAGE OF SINGLE GLOBAL VS. MULTIPLE LOCAL INDEPENDENT BOSONIC BATHS

The bath due to external or internal bosonic quasiparticles in solids, such as phonons, can be coupled to localized spins either as a single global bath for all spins; or many independent local baths, one for each localized spin. The latter choice was employed in the main text, as well as in numerous other studies [10–14]. It is well-justified in the context of atoms or ions trapped in optical lattices as simulators of quantum magnets[24], where each localized spins is far away from all others. This choice can still be valid even for solid-state magnetic materials realistically having only one common bosonic bath, as long as the bath relaxation is fast enough and/or if the correlation length of phonons is much larger than the lattice spacing of the material [11]. On the other hand, having a nonlocal coupling could enhance the dynamical generation of entanglement [25].

In this Section, we consider a single global bosonic bath interacting with localized spins within FI or AFI chain.

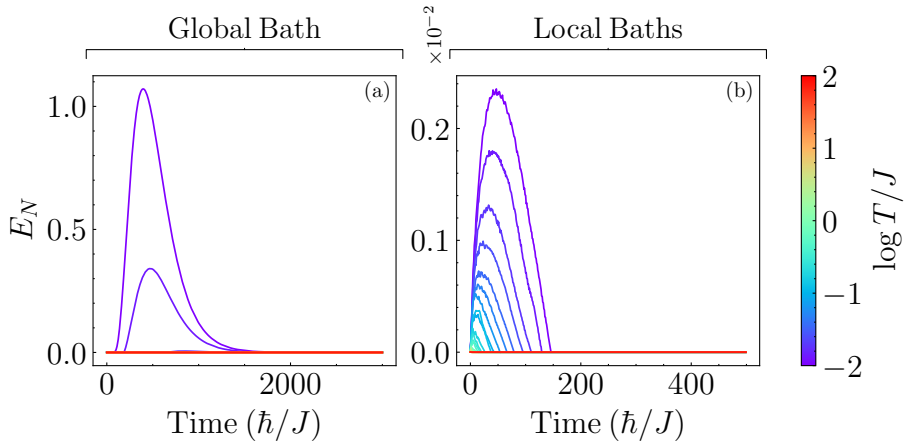

FIG. S5. Comparison of the Lindblad QME-computed entanglement negativity in FI chain of $N = 4$ sites hosting $S = 1/2$ localized spins which are coupled to: (a) a single global bosonic bath; or (b) many independent local bosonic baths, each coupled individually to a respective localized spin (as used also in the main text). The color of individual curves denotes different temperatures (color bar on the right) of bosonic baths in the units of Heisenberg exchange coupling J between the localized spins.

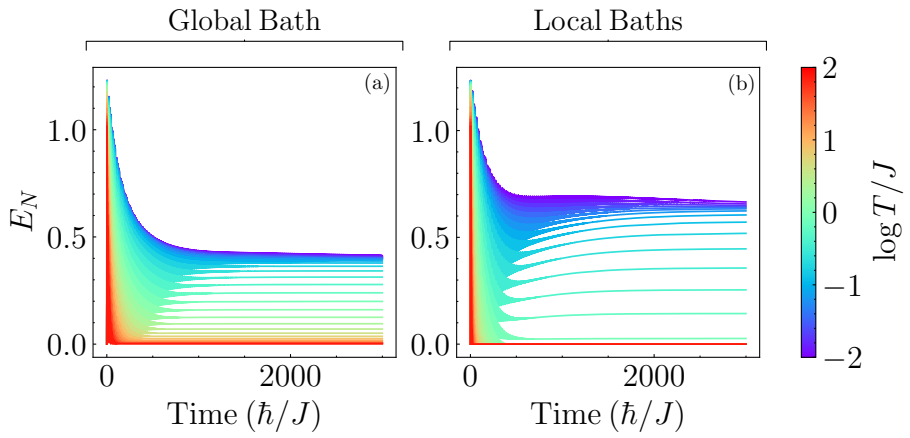

FIG. S6. The same information as in Fig. S5, but for AFI chain of $N = 4$ sites hosting $S = 1/2$ localized spins.

This requires to change the spins-bath coupling term in the main text to

$$\hat{V} = \sum_k g_k(\hat{a}_k + \hat{a}_k^\dagger) \cdot \sum_i \hat{\mathbf{S}}_i. \tag{7}$$

Figure S5 compares time dependence of entanglement negativity $E_N(t)$ for single global vs. many local independent bosonic baths coupled to localized spins within FI chain. While both types of system-bath coupling lead to unentangled state in the long-time limit, a considerably higher transient entanglement increase is obtained [Fig. S5(a)] in the case of a single global bath (note also that this is an example of transient "entanglement barrier" discussed in tensor network literature [26]). Nevertheless, quantum-to-classical transition in the case of FI is expected in both cases of system-bath coupling and in wide range of temperatures because entanglement eventually vanishes [Fig. S5]. In the AFI case [Fig. S6], there is little difference between two types of system-bath coupling—aside from the fact that a single global bath tends to maintain nonzero entanglement at higher temperatures, thereby enabling quantum-to-classical transition only when temperature is sufficiently high $T \gtrsim 2J$.

V. PROXIMITY OF STEADY-STATE SOLUTION OF LINDBLAD QME TO GIBBS DENSITY MATRIX

Standard derivations [17] of the Lindblad QME consider the bath correlation functions to satisfy the Kubo-Martin-Schwinger condition, thus ensuring that $\lim_{t\to\infty} \hat{\rho}(t) = \hat{\rho}_{\rm SS}$ becomes steady (i.e., time-independent) $\hat{\rho}_{\rm SS}$ in the long-time limit and properly transitions toward the canonical Gibbs density matrix $\hat{\rho}_{\rm SS} \equiv \hat{\rho}_{\rm th} = e^{-\beta\hat{H}}/{\rm Tr}(e^{-\beta\hat{H}})$ describing thermal equilibrium. However, the universal Lindblad QME [10] we employ in the main text is derived via a different route, so its steady-state can be slightly different from $\hat{\rho}_{\rm th}$, as intenesely discussed in recent literature [15, 16]. Nevertheless, this difference is well-bounded and can be further reduced using proper correction techniques [16].

In this Section, we use AFI case example from the main text computed fidelity between our steady state and Gibbs density matrix. Fidelity, measuring how close are two mixed quantum states to each other, between two arbitrary density matrices $\hat{\rho}_1$ and $\hat{\rho}_2$ is defined as [27]

$$F(\hat{\rho}_1, \hat{\rho}_2) = {\rm Tr}\left[\sqrt{\sqrt{\hat{\rho}_1}\hat{\rho}_2\sqrt{\hat{\rho}_1}}\right]^2 \tag{8}$$

where trivially $F(\hat{\rho}_1, \hat{\rho}_2) = 1$ for $\hat{\rho}_1 = \hat{\rho}_2$. The steady-state $\hat{\rho}_{\rm SS}$ for our example of AFI chain is computed by solving an algebraic equation

$$\hat{L}\hat{\rho}_{\rm SS} = 0, \;\; \hat{L}\hat{\rho} = -i[\hat{H}, \hat{\rho}] + \sum_i^{N_L} \hat{L}_i\hat{\rho}\hat{L}_i^\dagger - \frac{1}{2}\{\hat{L}_i^\dagger\hat{L}_i, \hat{\rho}\}, \tag{9}$$

where $\hat{L}$ is the Lindblad superoperator acting on the space of density matrices. Its fidelity [Fig. S7(a)] with the corresponding Gibbs density matrix $\hat{\rho}_{\rm th}$ reveals that at low temperatures there is a slight mismatch [orange dots

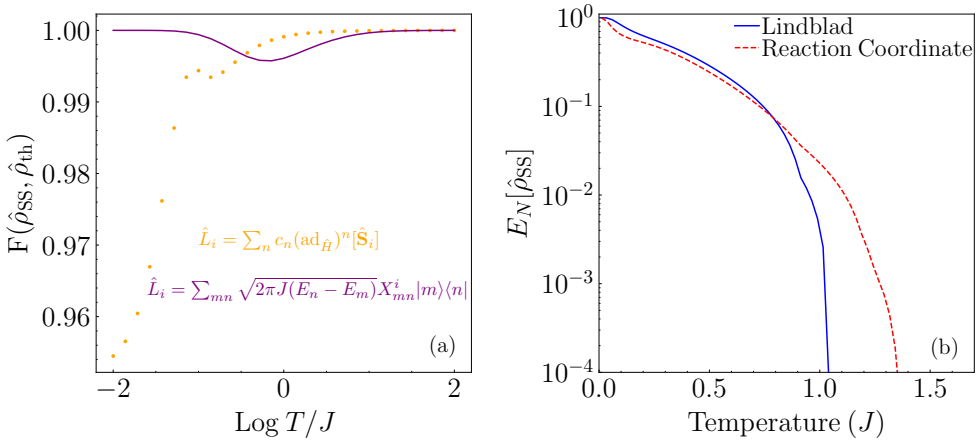

FIG. S7. (a) Fidelity [Eq. (8)] between steady-state solution $\hat{\rho}_{\mathrm{SS}}$ of universal [10] Lindblad QME, computed at time $t = 5000\hbar/J$ for our example of AFI chain composed of $N = 4$ sites hosting spins $S = 1/2$, and Gibbs density matrix $\hat{\rho}_{\mathrm{th}}$ describing thermal equilibrium state of the same system. Two different versions of Lindblad operators are considered: orange dots are obtained using Eq. (4) in the main text with truncation to the finite number of terms $N_L = 20$; and magenta line is obtained using the exact formula from Ref. [10]. (b) Entanglement negativity of steady state $\hat{\rho}_{\mathrm{SS}}$ computed at $t = 5000\hbar/J$ of time evolution by the Lindblad QME (blue solid line) vs. reaction-coordinate-based QME (red dashed line).

in Fig. S7(a)] between two mixed quantum states, $F(\hat{\rho}_{\mathrm{SS}}, \hat{\rho}_{\mathrm{th}}) < 1$, but this is actually an artifact of finite N_L truncating the series in Eq. (4) of the main text. This artifact can be removed by using the computationally more expensive expression for the Lindblad operators from Ref. [10], $L_i = \sum_{mn} \sqrt{2\pi J(E_n - E_m)} X^i_{mn} |m\rangle\langle n|$, where $|m\rangle$ is the eigenstate of the system Hamiltonian and $X^i_{mn} = \langle m|\hat{X}_i|n\rangle$ is the matrix element of the coupling operator between the system and the bosonic bath. Note that such an expression can only be used for a few localized spins, as it requires exact diagonalization of the system Hamiltonian in order to obtain its full eigenspectrum. The fidelity of steady-state computed by this second route and Gibbs density matrices is much closer to one [magenta line in Fig.S7(a)], but not exactly one as discussed extensively in recent literature [15, 16]. This proximity of steady-state solution of the Lindblad QME and Gibs density matrix provides a straightforward way to check whether quantum-to-classical transition, $\langle \hat{\mathbf{S}}_i \rangle(t) \mapsto \mathbf{S}_i(t)$, can be expected. That is, it is sufficient to compute entanglement negativity of $\hat{\rho}_{\mathrm{SS}}$ to see if such mixed quantum state will become unentangled or not in the long-time limit as *sine qua non* for quantum-to-classical transition.

In the case of strong system-bath coupling leading to non-Markovian dynamics, recent analyses [28] points out that $\hat{\rho}_{\mathrm{SS}}$ can be *far away* from Gibbs density matrix of the system, as the thermal state of joint system + bath is established. This is also the reason for strongly-coupled cases, studied in the main text using the "reaction coordinate" method [29] to obtain non-Markovian dynamics, *do not* lead to quantum-to-classical transition, $\langle \hat{\mathbf{S}}_i \rangle(t) \mapsto \mathbf{S}_i(t)$, within a wide interval of temperatures. Indeed, Fig. S7(b) confirms that entanglement negativity $E_N[\hat{\rho}_{\mathrm{SS}}]$ remains finite within a wider range of temperatures when using the "reaction coordinate" method and non-Markovian dynamics it generates [29] than in the case of Lindbladian dynamics.

VI. FINITE-SIZE DEPENDENCE OF ENTANGLEMENT NEGATIVITY

To confirm that our conclusions are independent of the system size, we compute entanglement negativity of steady-state solution [Sec. V], $E_N[\hat{\rho}_{\mathrm{SS}}]$, of the Lindblad QME in the example of AFI chain as a function [Fig. S8] of its number of sites $N = 6$–12 hosting localized spins $S = 1/2$. We extrapolate E_N into the thermodynamic limit $N \to \infty$ by plotting E_N vs. $1/N$ and by using a polynomial (of maximum degree 2) fit that extends toward $1/N = 0$ point. This procedure, executed in Fig. S8 for several bosonic bath temperatures, demonstrates that entanglement *remains finite* in the limit $N \to \infty$, as long as $T \lesssim J$. The fact that some of the fitting curves in Fig. S8 are even flat, i.e., independent of the system size, can be explained by the fact that system+bath is actually an infinite system already where repeated computation by increasing number of spins N is unnecessary, as observed in similar setting localized

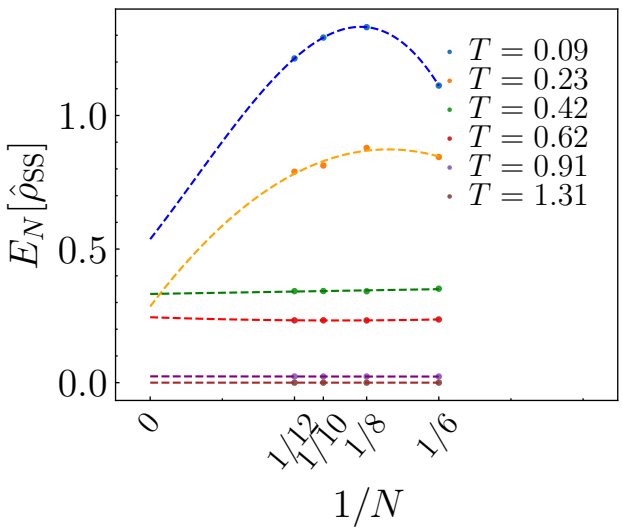

FIG. S8. Finite-size dependence of entanglement negativity of steady-state density matrix solution [Sec. V] of the Lindblad QME for AFI chain hosting $S = 1/2$ spins localized over $N = 6$–12 sites.

spins + dissipative-environment of prior studies [30].

[1] L. D. Landau and E. M. Lifshitz, On the theory of the dispersion of magnetic permeability in ferromagnetic bodies, Phys. Z. Sowjetunion **8**, 153 (1935).
[2] R. F. L. Evans, W. J. Fan, P. Chureemart, T. A. Ostler, M. O. A. Ellis, and R. W. Chantrell, Atomistic spin model simulations of magnetic nanomaterials, J. Phys. Condens. **26**, 103202 (2014).
[3] W. M. Saslow, Landau–Lifshitz or Gilbert damping? that is the question, J. Appl. Phys. **105**, 07D315 (2009).
[4] A. Szilva, Y. Kvashnin, E. A. Stepanov, L. Nordström, O. Eriksson, A. I. Lichtenstein, and M. I. Katsnelson, Quantitative theory of magnetic interactions in solids, Rev. Mod. Phys. **95**, 035004 (2023).
[5] R. P. Erickson, Long-range dipole-dipole interactions in a two-dimensional Heisenberg ferromagnet, Phys. Rev. B **46**, 14194 (1992).
[6] M. Sharma, Govind, A. Pratap, Ajay, and R. Tripathi, Role of dipole-dipole interaction on the magnetic dynamics of anisotropic layered cuprate antiferromagnets, Phys. Stat. Sol. B **226**, 193 (2001).
[7] E. Davis, B. Ye, F. Machado, S. Meynell, W. Wu, T. Mittiga, W. Schenken, M. Joos, B. Kobrin, Y. Lyu, Z. Wang, D. Bluvstein, S. Choi, C. Zu, A. Jayich, and N. Yao, Probing many-body dynamics in a two-dimensional dipolar spin ensemble, Nat. Phys. **19**, 836 (2023).
[8] B. Sbierski, M. Bintz, S. Chatterjee, M. Schuler, N. Y. Yao, and L. Pollet, Magnetism in the two-dimensional dipolar XY model, arXiv:2305.03673 (2023).
[9] R. E. Camley and K. L. Livesey, Consequences of the Dzyaloshinskii-Moriya interaction, Surf. Sci. Rep. **78**, 100605 (2023).
[10] F. Nathan and M. S. Rudner, Universal Lindblad equation for open quantum systems, Phys. Rev. B **102**, 115109 (2020).
[11] G. Schaller, F. Queisser, N. Szpak, J. König, and R. Schützhold, Environment-induced decay dynamics of antiferromagnetic order in Mott-Hubbard systems, Phys. Rev. B **105**, 115139 (2022).
[12] M. Weber, D. J. Luitz, and F. F. Assaad, Dissipation-induced order: The $s = 1/2$ quantum spin chain coupled to an Ohmic bath, Phys. Rev. Lett. **129**, 056402 (2022).
[13] T. Prosen, Exact nonequilibrium steady state of an open Hubbard chain, Phys. Rev. Lett. **112**, 030603 (2014).
[14] F. Queisser and R. Schützhold, Environment-induced prerelaxation in the Mott-Hubbard model, Phys. Rev. B **99**, 155110 (2019).
[15] J. S. Lee and J. Yeo, Comment on "Universal Lindblad equation for open quantum systems", arXiv:2011.00735 (2020).
[16] F. Nathan and M. S. Rudner, High accuracy steady states obtained from the universal Lindblad equation, arXiv:2206.02917 (2022).
[17] H.-P. Breuer and F. Petruccione, *The Theory of Open Quantum Systems* (Oxford University PressOxford, 2007).
[18] H.-P. Breuer, E.-M. Laine, J. Piilo, and B. Vacchini, Colloquium: Non-Markovian dynamics in open quantum systems, Rev. Mod. Phys. **88**, 021002 (2016).
[19] I. de Vega and D. Alonso, Dynamics of non-Markovian open quantum systems, Rev. Mod. Phys. **89**, 015001 (2017).

[20] J. L. García-Palacios and F. J. Lázaro, Langevin-dynamics study of the dynamical properties of small magnetic particles, Phys. Rev. B **58**, 14937 (1998).
[21] J. Zou, S. K. Kim, and Y. Tserkovnyak, Tuning entanglement by squeezing magnons in anisotropic magnets, Phys. Rev. B **101**, 014416 (2020).
[22] S.-K. Kim, Micromagnetic computer simulations of spin waves in nanometre-scale patterned magnetic elements, J. Phys. D: Appl. Phys. **43**, 264004 (2010).
[23] F. Iemini, D. Chang, and J. Marino, Dynamics of inhomogeneous spin ensembles with all-to-all interactions: breaking permutational invariance, arXiv:2309.10746 (2023).
[24] T. Brydges, A. Elben, P. Jurcevic, B. Vermersch, C. Maier, B. Lanyon, P. Zoller, R. Blatt, and C. Roos, Probing Rényi entanglement entropy via randomized measurements, Science **364**, 260 (2019).
[25] A. Seif, Y.-X. Wang, and A. A. Clerk, Distinguishing between quantum and classical Markovian dephasing dissipation, Phys. Rev. Lett. **128**, 070402 (2022).
[26] A. Lerose, M. Sonner, and D. A. Abanin, Overcoming the entanglement barrier in quantum many-body dynamics via space-time duality, Phys. Rev. B **107**, L060305 (2023).
[27] M. A. Nielsen and I. L. Chuang, *Quantum Computation and Quantum Information: 10th Anniversary Edition* (Cambridge University Press, 2010).
[28] J. D. Cresser and J. Anders, Weak and ultrastrong coupling limits of the quantum mean force Gibbs state, Phys. Rev. Lett. **127**, 250601 (2021).
[29] G. B. Cuetara, M. Esposito, and G. Schaller, Quantum thermodynamics with degenerate eigenstate coherences, Entropy **18**, 447 (2016).
[30] A. Schuckert, A. Orioli, and J. Berges, Nonequilibrium quantum spin dynamics from two-particle irreducible functional integral techniques in the Schwinger boson representation, Phys. Rev. B **98**, 224304 (2018).